Crystallization of triethyl-citrate-plasticized poly(lactic acid) induced by chitin nanocrystals

*Shikha Singh,[a,b] Maria Lluisa Maspoch[b] and Kristiina Oksman[a,c]**

[a] University of Technology, SE-97 187 Luleå, Sweden

[b]Centre Català del Plàstic (CCP), Universitat Politècnica de Catalunya Barcelona Tech (ETSEIB-UPC), Pavellò G, Planta 1, Avenida Diagonal, 647, Barcelona 08028, Spain

[c]Fibre and Particle Engineering, University of Oulu, FI-90014 Oulu, Finland

*Correspondence to: Kristiina Oksman (E-mail: Kristiina.oksman@ltu.se)

ABSTRACT: The aim of this study was to gain a better understanding of the crystallization behavior of triethyl-citrate-plasticized poly(lactic acid) (PLA-TEC) and the influence of chitin nanocrystals (ChNCs) on this crystallization.. The isothermal crystallization behavior of PLA-TEC was studied by polarized optical microscopy (POM), scanning electron microscopy (SEM), differential scanning calorimetry (DSC), and X-ray diffraction (XRD). Interestingly, the addition of just 1 wt% ChNCs increased the crystallization rate in the temperature range of 135–125 °C. The microscopy studies confirmed the presence of at least three distinct types of spherulites: negative, neutral, and ring-banded. The ChNCs also increased the degree of crystallinity (by up to 32%), even at a fast cooling rate of 25 °C/min. The XRD studies further revealed the nucleation effect induced by the addition of ChNCs and thus explained the faster crystallization

rate. To conclude, the addition of a small amount (1 wt%) of ChNC to plasticized PLA significantly affected its nucleation, crystal size, crystal type, and crystallization speed; therefore, the proposed route can be considered suitable for improving the crystallization behavior of PLA.

KEYWORDS. Poly(lactic acid), plasticizer, chitin nanocrystals, isothermal crystallization, microstructure.

INTRODUCTION

Poly(lactic acid) (PLA) is a promising biobased, biodegradable, nontoxic, and commercially available thermoplastic polymer that is manufactured from natural resources (*e.g.*, corn and sugar beets)[1]. Furthermore, PLA has good mechanical properties (high stiffness and tensile strength), good optical properties (high transparency), and moderate barrier properties. However, PLA is brittle, and it has a low melt strength and slow crystallization rate[1]. The mechanical and barrier properties of PLA are highly dependent on its morphology and crystallinity[2]. The slow crystallization rate of PLA results in low crystallinity, which consequently limits its use in industrial applications[3]. Therefore, studies on improving the crystallization are crucial and fundamental aspect which need to be addressed.

One approach to enhance the crystallization of PLA is through the addition of plasticizers[4]. Plasticizers promote the growth rate of crystallites[5] and act as processing aids[6]; they also enhance the flexibility and ductility of polymer materials[4]. Triethyl citrate (TEC) is a biodegradable, nontoxic, and efficient plasticizer for PLA[7]. However, TEC also has some drawbacks is that it degrade the thermal[8], optical[9], and mechanical properties[10] of PLA.

Another approach is to use nanosized additives and reinforcements; because of their large surface area, they can act as effective nucleating agents and promote the crystallization of

polymers[11]. Several inorganic additives/reinforcements such as clays (*e.g.*, montmorillonite[12], silica[13], and halloysite nanotubes[14]) and carbon-based materials (*e.g.*, carbon nanotubes[2] and graphene[15]) have been widely used in nanocomposites. However, the poor biodegradability and toxicity of some of these materials restrict their use in food packaging applications. Therefore, the use of polysaccharide-based reinforcements would be more beneficial not only because of their biodegradable nature, low toxicity, low cost, and easy availability[16] but also because of their role as better nucleating agents. The most commonly used nanoadditives are nanocelluloses[17] and starch nanoparticles[18]. For example, Mathew *et al.*[17] studied the crystallization of PLA in the presence of three different types of cellulose reinforcements: microcrystalline cellulose, cellulose fibers, and wood flour. They found that the crystallization temperature influences both the number and size of the spherulites. Gray[19] investigated the crystallization of polypropylene (PP) on the surface of cellulose nanocrystals (CNCs); in the study, he employed CNC acted as a nucleating agent and a transcrystalline layer (TCL) of PP was formed around the CNC film. The CNCs were found to increase the crystallization of PP. Pei *et al.*[11] studied the crystallization of PLA in the presence of CNCs. The CNCs were functionalized with silane to improve their dispersion in the PLA matrix, and their role as nucleating agents was explained. The results showed that the crystallization rate was improved by the addition of 1 wt% silane-functionalized CNCs (SCNCs); this improvement was attributed to their stronger nucleating ability compared to that of non-modified CNCs. The degree of crystallinity improved from 14% (PLA) to 30% (PLA-SCNCs). Sullivan *et al.*[20] investigated the crystallization of PLA films prepared by melt compounding with different CNC contents (1 wt%, 2 wt%, and 3 wt%). They found that the crystallinity of the PLA film improved from 11% to 30% by the addition of 3 wt% CNCs. Trifol *et al.*[21] studied acetylated cellulose nanofibers

(CNFs), CNCs, and clay (C30B) as additives for PLA nanocomposites. They observed that the addition of just 1 wt% CNFs and 1 wt% CNCs significantly improved the crystallization kinetics of PLA without affecting its transparency. They explained that the improved crystallinity could be a result of better nucleation abilities of the CNFs and CNCs than that of the nanoclay. Furthermore, the added CNCs provided better crystallinity than the added CNFs.

The crystallization of PLA in the presence of various natural nanomaterials has been studied; however, the potential use of chitin nanocrystals (ChNCs) for this crystallization improvement has been explored to a lesser extent than that of CNCs. ChNCs are natural polymers that are generally found in the exoskeleton of arthropods (crustaceans and mollusks)[22]. ChNCs have low density, nontoxicity, biodegradability, and biocompatibility[22]. In addition to possessing good mechanical and thermal properties, ChNCs exhibit anti-microbial properties; as a result, they can possibly be used as nanoreinforcements in packaging applications, especially food packaging.

In the present study, the isothermal crystallization of plasticized PLA in the presence of ChNCs was studied. The main objective was to study the nucleation abilities of ChNCs and their effects on the crystallization rate and spherulite morphology. Thin films of neat PLA, plasticized PLA, pure ChNCs, and PLA-TEC-ChNC nanocomposites were prepared and their crystallization kinetics, crystallinity, and crystal size, as well as the spherulite morphology, were examined by differential scanning calorimetry (DSC), X-ray diffraction (XRD), polarized optical microscopy (POM), and scanning electron microscopy (SEM).

EXPERIMENTAL

Materials. High-molecular-weight PLA in the form of pellets, which was provided by FUTERRO (Escanaffles, Belgium), was used as a matrix polymer in the composites and as a

reference material for the crystallization studies. The melt flow index (MFI) of the received PLA was 8 g/10 min (190 °C, 2.16 kg) and its L-isomer content was 99%, according to the supplier. TEC in liquid form (≥99% with Alfa Aesar), molecular weight of 276.3 g/mol, purchased from WVR, Sweden, was used as the plasticizer.

ChNCs were used as the nanoadditives in the plasticized PLA; these nanocrystals were expected to affect the crystallization rate of PLA. PLA-ChNC nanocomposites were prepared using TEC as a processing aid for the compounding process as well as to enhance the dispersion of the ChNCs in the PLA matrix; further details of this preparation have been provided in our previous study[23]. The material compositions and sample codes are listed in Table 1. The composition of the PLA-TEC-ChNC nanocomposite material (in wt%) was 79:20:1. PLA-TEC-ChNC nanocomposites have been described in detail in our previous studies[7,24]. In brief, the ChNCs were prepared by acid hydrolysis of a purified chitin powder. The ChNCs were subjected to POM and AFM observations. POM image shows the birefringence of ChNCs and the AFM image shows the dimensions of the ChNCs. The size distribution of the ChNCs was calculated from the height image; the obtained data are shown in Figures 1 (b) and (c). For this calculation, a line was drawn across the height image by using Gwyddion software and the peak profiles of the crystals were extracted. Several lines were drawn to include as many as crystals visible in the image as possible. Then, histograms of the size distributions were plotted and the ChNC dimensions were calculated. The height and length of the ChNCs were 2–22 nm and 8–38 nm, respectively.

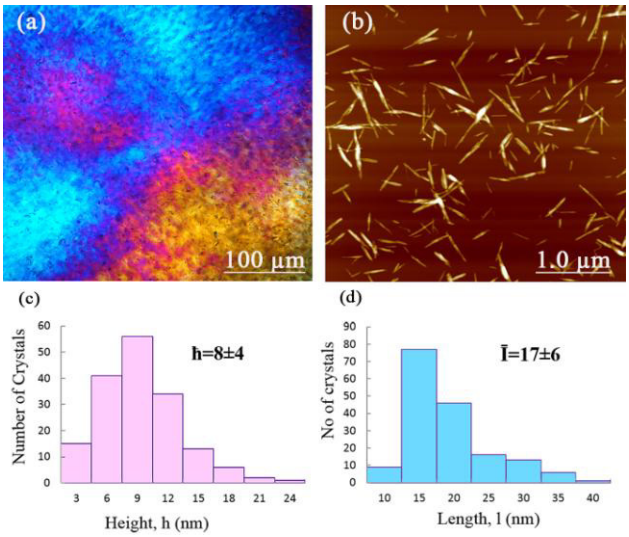

Figure 1. (a) POM image of ChNCs, showing their birefringence, and (b) AFM image of ChNCs, showing their needle-like structure. (c) Average diameter and (d) length of used ChNCs.

Table 1. Sample codes and compositions of prepared materials (wt%).

Materials	PLA	TEC	ChNC
PLA	100	0	0
PLA-TEC	80	20	0
PLA-TEC-ChNC	79	20	1

Preparation of ChNC films. Pure ChNC films were prepared by solution casting, after which the aqueous suspension of ChNCs (19.5 wt%) was evaporated and dried overnight in an oven at 80° C. The thickness of the obtained films was measured using a digital micrometer (Mitutoyo, Japan); it was in the range of 20–40 µm. These films were used to better understand transcrystalline transformation. In order to observe this transformation, the films were

positioned as reported in the study of Gray *et al.*[19]. A thin film of ChNCs was inserted between PLA films and observed by POM, as shown in Figure 2.

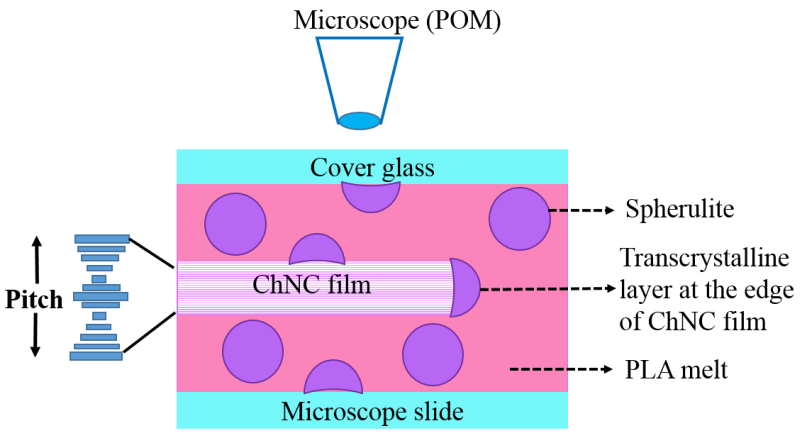

Figure 2. Schematic representation showing manner of insertion of ChNC film between PLA films in POM study.

Preparation of films of PLA-based materials. Pellets of neat PLA, PLA-TEC, and the PLA-TEC-ChNC nanocomposite were compression-molded between steel plates to obtain films. Small amounts (2 g) of the pellets were first kept at 190 °C for 2 min under contact pressure, and after they melted, the pressure was increased from 0 to 10 MPa in 1 min. The films were subsequently cooled in air. The film thickness ranged between 20 µm and 40 µm.

Polarized optical microscopy (POM). The Nikon Eclipse MA200 (Japan) polarized optical microscope equipped with the Linkam THM600 (UK) hot stage and temperature controller was used for examining the isothermal crystallization of the prepared materials. Objectives with 10X and 20X magnifications were used. A piece of the film was squeezed between two glass slides and transferred to the hot stage. Prior to crystallization, the sample was heated to 200 °C to eliminate any previous thermal history and then cooled at a rate of 25 °C/min to three specific

temperatures, 135 °C, 130 °C, and 125 °C; finally, the sample was isothermally crystallized for 30 min. These temperatures were selected because PLA shows a rapid transition in this temperature range (135–125 °C)[25]. The polarized optical micrographs of the sample were recorded using a charge-coupled device (CCD) camera at various time intervals.

Atomic force microscopy (AFM). The size distribution of the ChNCs were determined by AFM; a Veeco Multimode Scanning Probe (USA) with tapping mode. The length and width of the ChNCs were analyzed by Gwyddion software.

Scanning electron microscopy (SEM). The surface morphologies of the TCL and the spherulites formed in the presence of the ChNC films and PLA-TEC-ChNC films were examined using a SEM apparatus (JEOL, JSM-6460LV, Japan) after the isothermal crystallization processes. To examine the transcrystalline morphology of the materials, the samples were etched with NaOH and ethanol (1:2 by volume). The etched surface was washed with distilled water. The film was rinsed 2–3 times with distilled water. The surfaces of these etched samples were then coated with gold by sputtering, and the acceleration voltage was kept at 5 kV.

Differential scanning calorimetry (DSC). The Mettler Toledo DSC 822e (Switzerland) instrument was used to study how the addition of TEC and ChNCs affected the thermal properties and crystallization of PLA-TEC. Samples were placed in an aluminum pan, and then, the analysis were performed under a nitrogen atmosphere. The materials were isothermally crystallized in five steps.

1. The sample was heated from -20 °C to 200 °C at a heating rate of 10 °C/min.
2. The sample was isothermally annealed at 200 °C for 5 min in order to eliminate any previous thermal history[2].

3. The sample was cooled to the isothermal crystallization temperature (*e.g.*, 125 °C) at a cooling rate of 25 °C/min.
4. Isothermal crystallization was performed for 30 min.
5. The sample was reheated from 125 °C to 200 °C at a heating rate of 10 °C/min in order to measure the melting endotherm.

The glass transition temperature (T_g), melt temperature (T_m), cold crystallization temperature (T_{cc}), and heat of melting (H_m) of all the samples were determined, and the percentage crystallinity corresponding to each curve was calculated. The percentage crystallinity was determined using the following empirical equation[17]:

$$Crystallinity\ (\%) = \frac{\Delta H_m - \Delta H_c}{93.1} \times 100 \qquad (1)$$

where ΔH_m is the melting enthalpy, ΔH_c is the cold crystallization enthalpy, and the constant 93.1 (unit: J/g) corresponds to the ΔH_m value for 100% crystalline PLA[17].

X-ray diffraction (XRD). The effect of ChNCs on the crystallization of PLA was investigated using a PANalytical Empyrean diffractometer (Almelo, The Netherlands) with Cu-Kα radiation (λ = 1.5405 Å). Prior to the XRD measurements, the materials were isothermally crystallized in a manner similar to that in the previous experiments (at 125 °C for 30 min). The measurements were performed at an acceleration voltage and current of 45 kV and 40 mA, respectively, for 1 h over a 2θ range of 5°–60° (step size: 0.026°). Further investigation of the crystal size of the materials was performed using the Scherrer equation[27]:

$$\frac{K\lambda}{BCos\ (\theta)} \qquad (2)$$

Here, L is the crystal size (crystalline lamella thickness); K is the dimensional shape factor, also known as the Scherrer constant; λ is the radiation wavelength; B is the full width at half-maximum (FWHM) value of different peaks; and θ is the Bragg angle.

Fourier transform infrared (FTIR) spectroscopy. FTIR spectroscopy was performed to further analyze the effect of addition of ChNCs to PLA-TEC and to observe the interactions of the PLA matrix with TEC and the ChNCs in the PLA-TEC-ChNC nanocomposites. A VERTEX 80 (Bruker, Billerica, MA, USA) FTIR spectrophotometer with a range of 400–4000 cm^{-1} and a 128-scan resolution was used for the analysis. All samples were characterized by the KBr pellet method. According to this method, 0.03 mg of materials were mixed and ground with powdered KBr to make pellets, and the obtained pellets were used for further studies.

RESULTS AND DISCUSSION

Effect of TEC plasticizer on crystallinity. Figure 3 shows the results of POM studies of the effect of the TEC plasticizer on the crystallization of PLA at the three crystallization temperatures of 135 °C, 130 °C, and 125 °C. As the first step, the material was cooled from the melt state to 135 °C and kept at this temperature for 5 min, 10 min, and 15 min. The crystallization rate was found to be very slow, and only a few spherulites were visible on the interface between PLA and PLA-TEC; these spherulites grew slightly with increase in time. When the crystallization temperature was decreased to 130 °C, nucleation already began to occur more noticeably at the interface after 5 min, and after 15 min, a TCL was formed and some large spherulites were visible in the plasticized PLA. However, almost no spherulites were observed in the PLA film. At the lowest temperature, *i.e.*, 125 °C, crystallization initially occurred at the interface and spherulites inside PLA-TEC underwent nucleation at 5 min. At 10 min, the heterogeneous nucleation improved, which resulted in the formation of the TCL; at 15 min, the TCL became more prominent. Both

bulk nucleation and heterogeneous nucleation occurred rapidly at this temperature, and consequently, the number of spherulites increased. Small spherulites were formed at 15 min at the crystallization temperature of 125 °C, and the size of spherulites at this temperature was smaller than that at 130 °C; this result indicated that temperature influences the spherulite size. The spherulites were observed to have a typical Maltese-cross pattern spherulites[28] with negative birefringence[29] at this temperature. Some small spherulites were also formed at the periphery of the larger ones.

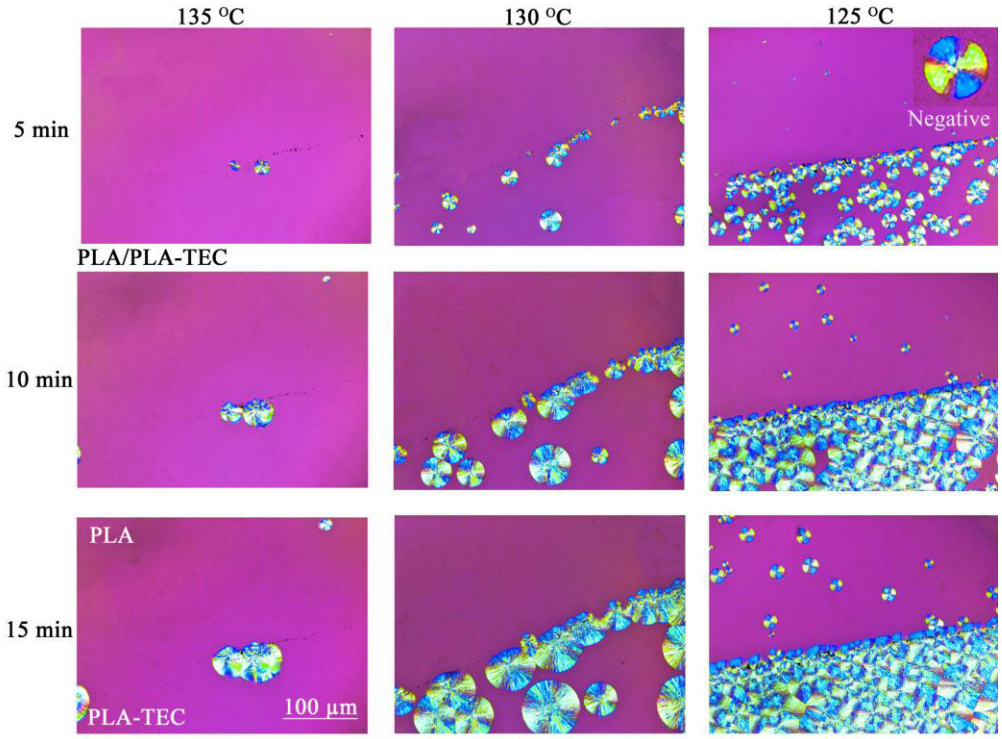

Figure 3. Comparison of isothermal crystallizations of neat PLA and PLA-TEC at different temperatures (135 °C, 130 °C, and 125 °C) and holding times of 5 min, 10 min, and 15 min.

Isothermal crystallizations of PLA-TEC and PLA-TEC-ChNC nanocomposite. Figure 4 shows a comparison of the isothermal crystallizations of plasticized PLA-TEC and the PLA-TEC-ChNC

nanocomposite at 135 °C, 130 °C, and 125 °C after 30 min. It is seen that when the temperature was decreased to 135 °C, the nucleation of the nanocomposites was stronger than that of PLA-TEC because of the presence of ChNCs in the former. When the temperature was decreased further to 130 °C, the nucleation of the nanocomposite improved greatly. Interestingly, at 130 ° C, multi-ring-banded spherulites were formed in the plasticized PLA-TEC. At 125 °C, nucleation occurred very rapidly in the PLA-TEC-ChNC nanocomposite and the spherulites were smaller than those in the plasticized PLA-TEC.

The overall rate of crystallization of PLA was faster at 125 °C than at 130 °C and 135 °C. Comparison of the crystallization of PLA-TEC with that of the PLA-TEC-ChNC nanocomposite clearly reveals that the crystallization rate of the PLA-TEC-ChNC nanocomposites was higher and the size of spherulites in this nanocomposite were smaller. This enhanced crystallization of the PLA-TEC-ChNC nanocomposite is because the ChNCs act as a nucleating agent and the plasticizing effect of the TEC present in the nanocomposite increases the growth rate of the crystalline superstructure, which, in turn, facilitates or accelerates the folding necessary for the formation of the lamellae (which are the basic crystalline units that constitute a spherulite).

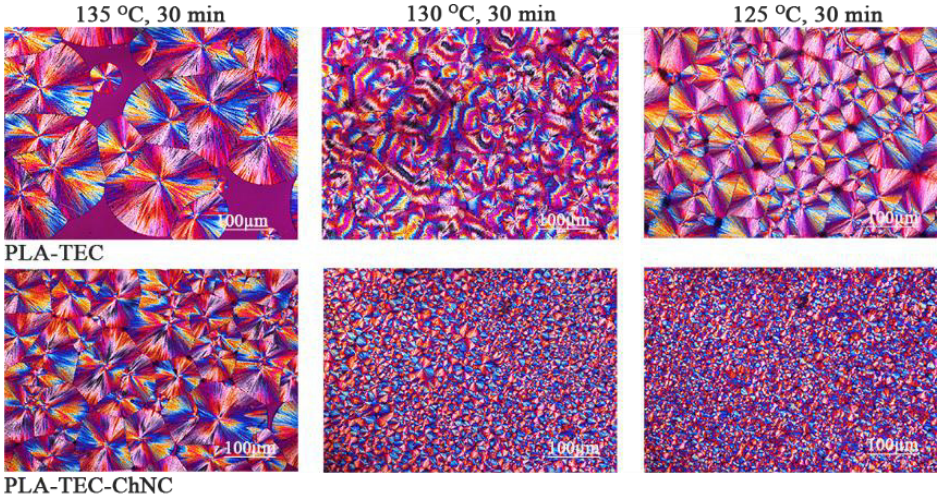

Figure 4. Comparison of isothermal crystallizations of PLA-TEC and PLA-TEC-ChNC nanocomposite at 135 °C, 130 °C, and 125 °C after 30 min.

Further crystallization of PLA-TEC was performed in the presence of a thin film of the PLA-TEC-ChNC nanocomposite, as shown in Figure 5. The crystallization rate of PLA improved. Both bulk nucleation (which refers to nucleation that occurs in all directions, especially inside the PLA-TEC-ChNC film) and heterogeneous nucleation also improved, as is clearly revealed by the growth of a larger number of spherulites in Figure 5. Initially, the crystallization was performed at 135 °C, and more spherulites were visible inside the PLA-TEC-ChNC film at this temperature. Figure 5 also shows that the ChNCs induced an increase in the overall rate of crystallization of PLA-TEC. Then, the crystallization was performed at 130 °C, and the rate of bulk nucleation improved further at this temperature. Most importantly, multi-ring-banded spherulites were observed at this crystallization temperature. Finally, crystallization was performed at 125 °C. At this temperature, bulk nucleation occurred at an extremely rapid rate, even at 5 min. The formed TCL was clearer after 5 min, and at 15 min, the surface of the PLA-TEC-ChNC film was almost fully covered with the spherulites. In addition to negative type spherulites, some neutral types were also observed at this temperature.

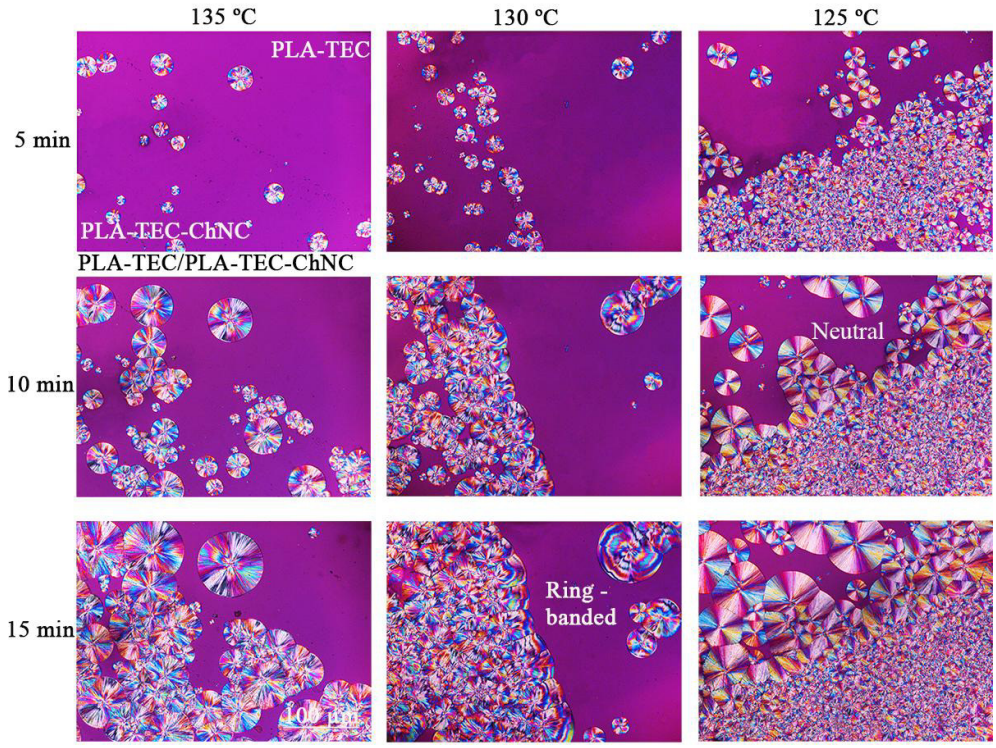

Figure 5. Comparison of crystallizations of PLA-TEC and PLA-TEC-ChNC nanocomposite at 135 °C, 130 °C, and 125 °C for holding times of 5 min, 10 min, and 15 min.

Figure 6 shows that spherulites of a very specific type, *i.e.*, multi-ring-banded spherulites, appeared at 130 °C. The number of rings inside a spherulite increased with increase in time from 5 min to 30 min. At 5 min, the rings were not clear, but at 10 min, the rings were visible; further layering of rings was observed at 15 min. The number of rings increased up to 25 min, after which their growth was restricted by the formation of smaller spherulites on the surface of the larger ones. These numerous smaller spherulites were formed because the ChNCs acted as a heterogeneous nucleating agent. Figure 7 (a) shows the spherulite radius as a function of time; specifically, this plot depicts how the radius of spherulites increases with time. The plot is an almost straight line. Jing *et al.*[30] reported observation of similar behavior; they observed that the

radius of spherulites increased linearly with the crystallization time. Figure 7 (b) shows a plot of the position of the spherulite bands versus their height; this plot reveals an almost regular pattern.

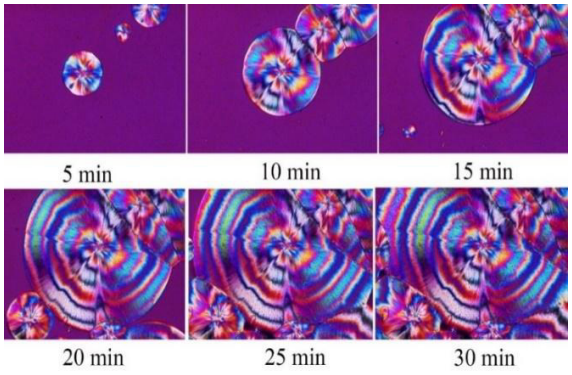

Figure 6. Multi-ring-banded spherulites formed at 130 °C. The figure depicts how the number of rings of spherulites increases with time (5–30 min).

Banding is usually observed in chiral polymers such as PLA, which consist of an asymmetric carbon atom in the backbone. In the case of PLA, banding can only be observed at temperatures above 110 °C, usually over a range of ±5–10 °C[28]. This banding of PLA is linked to polymorphism[28].

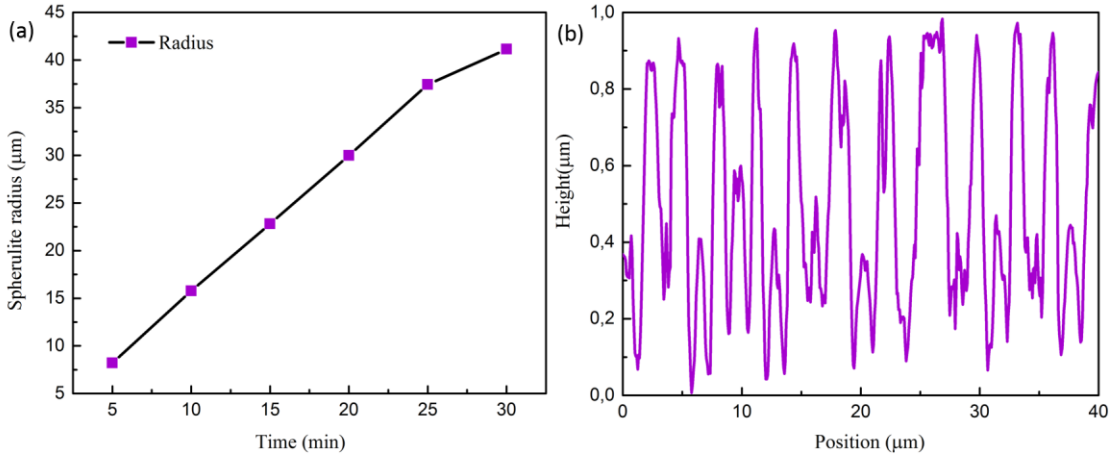

Figure 7. (a) Spherulite radius (ring-banded spherulite) as a function of time during isothermal crystallization at 130 °C. (b) Plot of position of spherulite bands versus their height.

Ring-banded spherulites. Formation of ring-banded spherulites is a common occurrence in semicrystalline polymers[28]. Lamellar twisting in banded spherulites accelerates in the presence of nucleating agents and enhances the regularity of the bands. In this study, ring-banded spherulites of PLA were observed at 130 °C. The possible mechanism of formation of the ring-banded spherulites in the PLA-TEC-ChNC film is shown in Figure 8. During the crystallization of PLA, the PLA chains folded together in the presence of TEC and the ChNCs (Figure 8), and consequently, PLA lamellae were formed (Figure 8 (b)). The PLA lamellae finally twisted (Figure 8 (c)), which resulted in the formation of ring-banded spherulites (Figure 8 (d)).

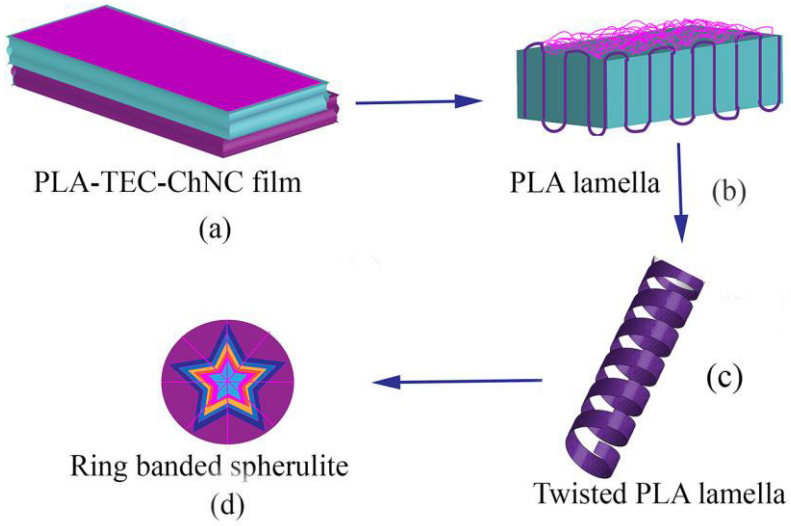

Figure 8. Possible mechanism of formation of ring-banded spherulites during crystallization of PLA.

Effect of pure ChNC film on crystallization of PLA-TEC. Figure 9 shows the crystallization of PLA-TEC in the presence of the pure ChNC film. Crystallization was first performed at 135 °C; at this temperature, nucleation occurred mainly at the interface between the ChNCs and the PLA-TEC film, which indicated the good nucleation ability of the ChNCs. The number and size of the spherulites increased after 10 min, and a very prominent TCL was observed after 15 min. When

the crystallization temperature was decreased to 130 °C, both bulk nucleation and heterogeneous nucleation improved and spherulites were observed in the vicinity of the ChNC film. Notably, ring-banded spherulites were also observed at 130 °C, and the TCL was thicker than that observed at 135 °C. When further crystallization was performed at 125 °C, the bulk nucleation improved greatly and numerous spherulites were observed inside the PLA-TEC film.

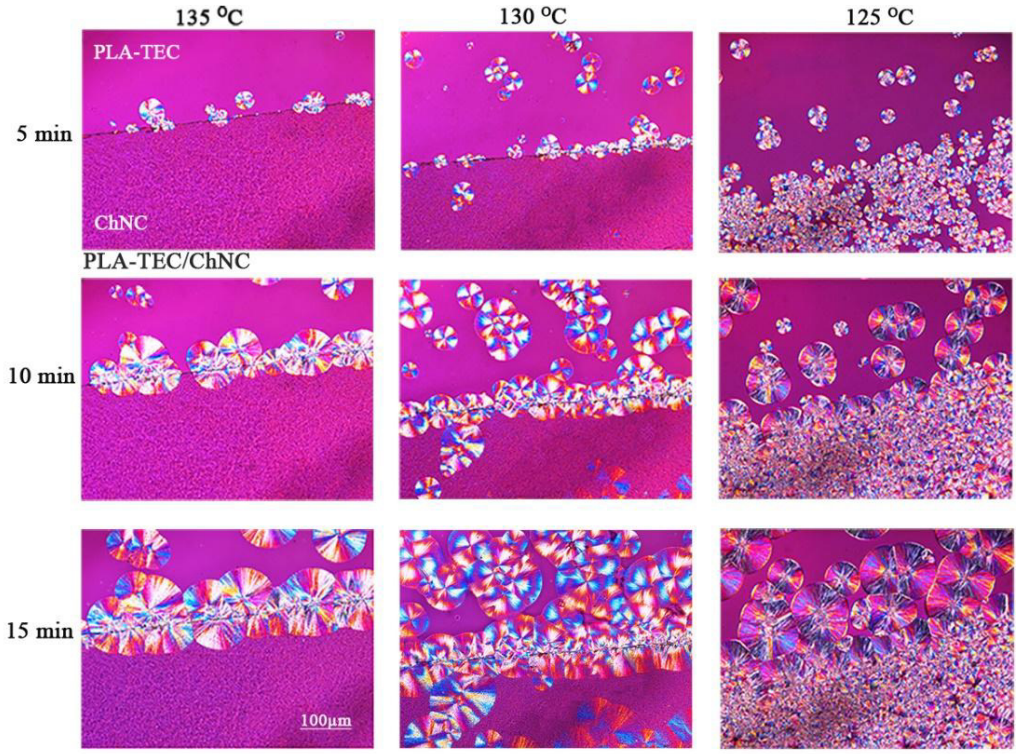

Figure 9. Crystallization of plasticized PLA-TEC in the presence of pure ChNC film at (a) 135 ° C, (b) 130 °C, and (c) 125 °C, for holding times of 5 min, 10 min, and 15 min.

Evaluation of surface morphology and lamellar arrangements of spherulites. SEM studies were conducted to better understand the surface morphology of the TCLs and the lamellar arrangements of spherulites formed during the isothermal crystallization of PLA-TEC film. Figure 10 shows the SEM images of the surface of the PLA-TEC film and the spherulites formed in the presence of PLA-TEC-ChNC film and pure ChNC film. In both the cases, PLA-TEC film

was considered as a matrix. In the cases of the pure ChNC film and PLA-TEC-ChNC film, the ChNCs acted as a nucleating agent and TEC improved the growth of crystals. As shown in Figures 10 (a) and (b), an interesting TCL is observed on the surface of the PLA-TEC-ChNC film, wherein the lamellae grow radially near the PLA-TEC-ChNC film and are organized in such a manner that they form a fan-shaped hemispherical structure. In Figures 10 (c) and (d), a fan-shaped TCL is also visible on the surface of the pure ChNC film. The TCL on the PLA-TEC-ChNC film is more strongly textured than that on the pure ChNC film.

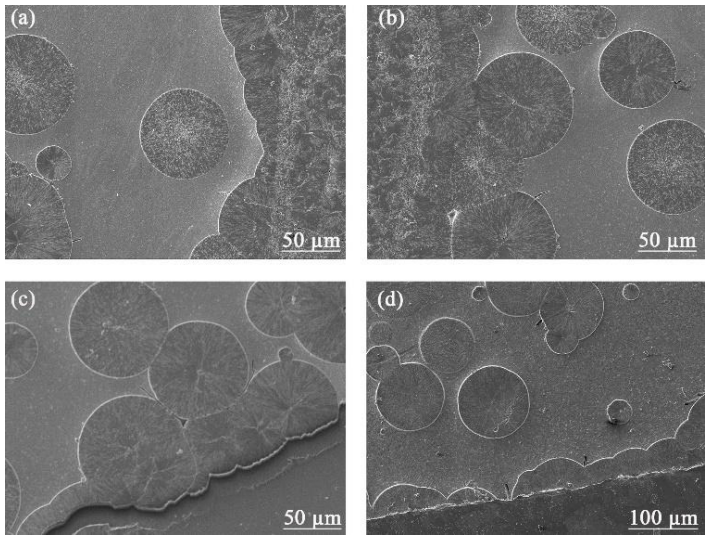

Figure 10. Surface morphology of PLA-TEC (a), (b) PLA-TEC-ChNC film and (c), (d) pure ChNC film, after isothermal crystallization at 125 °C.

Further examination revealed the different types of spherulites. Figures 11 (a)–(c) show the lamellar structures of the different types of spherulites formed on the surface of the PLA-TEC-ChNC nanocomposite. It can be seen from Figure 11 (a) that the lamellae in the spherulites are oriented such that they form a ring inside the spherulites. Specifically, the circular fibrous texture of the lamellae leads to the formation of a circular ring within the periphery of the spherulites. However, the type of lamellar pattern of the spherulites as observed in Figure 11 (b) is slightly

different from that observed in Figure 11 (a): the lamellae are observed to grow radially in Figure 11 (b). A completely different type of lamellar pattern of the spherulites—a scattered lamellar pattern—is observed in Figure 11 (c). Nimah *et al.*[31] reported a similar type of lamellar pattern for the spherulites of PLA. Both the POM and the SEM observations revealed that these different types of spherulites have different lamellar arrangements.

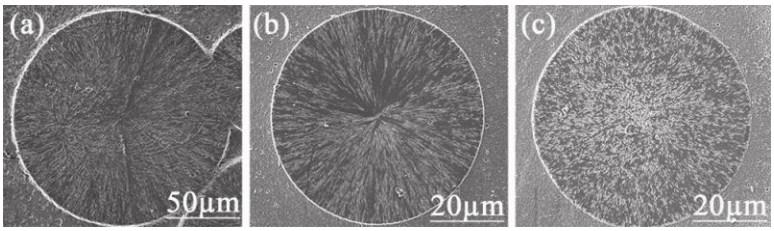

Figure 11. Different types of spherulites formed during isothermal crystallization of PLA-TEC on the surface of PLA-TEC-ChNC nanocomposite: (a) circular fibrous spherulites, (b) banded spherulites, and (c) spherulites with scattered lamellar pattern.

Thermal analysis. DSC measurements were performed to estimate the glass transition temperature (T_g), melt temperature (T_m), and cold crystallization temperature (T_{cc}); the measurement results are listed in Table 2. The DSC curve of PLA showed T_g, T_{cc}, and T_m at 62 °C, 101 °C, and 174 °C, respectively, which are typical of semicrystalline polymers and similar to values reported in the literature[32]. The addition of TEC to PLA lowered the T_g, T_{cc}, and T_m values of PLA to 34 °C, 68 °C, and 163 °C, respectively. This lowering of T_g, T_{cc}, and T_m of PLA is attributed to the plasticizing effect of the plasticizer, *i.e.*, TEC[9]. Maiza *et al.*[4] reported the same trend in their study of the plasticizing effect of TEC on the properties of PLA; they observed that T_g decreased with an increase in the TEC content. The reduction in the T_g, T_m, and T_{cc} of PLA with the addition of TEC were due to the higher flexibility of the polymer chains in the presence of plasticizers[33]. However, the incorporation of 1 wt% ChNCs into PLA-TEC did not lower the

T_g, T_{cc}, and T_m of PLA as much as the addition of TEC did; these temperatures were 37 °C, 73 °C, and 166 °C, respectively, after the incorporation of ChNCs. Li *et al.*[34] also found that the addition of chitin nanowhiskers (ChNWs) did not lower the T_g, T_{cc}, and T_m of PLA; the T_g, T_{cc}, and T_m of PLA before the addition of ChNWs were 59.5 °C, 101.9 °C, and 171.9 °C, respectively, and those after the addition of ChNWs were (depending on the added ChNW content) 58.8–57.8 °C, 101.3–98.3 °C, and 171.7–167.9 °C, respectively. The reduction in the T_g, $T_{cc,}$ and T_m of the PLA-TEC-ChNC nanocomposite (see Table 2) may be because of the plasticizing effect of TEC.

Table 2. Glass transition temperature (T_g), melt temperature (T_m), cold crystallization temperature (T_{cc}), heat of melting (H_m), and percentage crystallinity.

Materials	T_g(°C)	T_{cc}(°C)	T_m(°C)	δ H_m(J/g)	Crystallinity (%)
PLA	62	101	174	34.9	14.4
PLA-TEC	34	68	163	39.3	24.6
PLA-TEC-ChNC	37	73	166	42.3	32.0

Figure 12 shows the DSC traces of the second melting peaks of PLA, PLA-TEC, and the PLA-TEC-ChNC nanocomposite obtained after their isothermal crystallization for 30 min. An almost negligible double melting peak was observed for PLA. However, rather broad second melting peaks were observed for PLA-TEC and the PLA-TEC-ChNC nanocomposite. The melting peaks of PLA-TEC and the PLA-TEC-ChNC nanocomposite were shifted toward lower temperatures in comparison to that of PLA. The spikes in the second melting peak of the PLA-TEC-ChNC nanocomposite were extremely prominent. These prominent peaks are ascribed to the faster crystallization rate of PLA in the PLA-TEC-ChNC nanocomposite. Moreover, formation of the

double melting peak indicated different crystal morphology of PLA[15]. This shift in the melting peaks of PLA with the addition of TEC and ChNCs indicated the occurrence of some interaction of TEC and the ChNCs within the PLA chain. Muller *et al.*[35] studied the influence of poly(ethylene glycol) (PEG) on the crystallization and thermal behavior of PLA and found that PEG interacted with the PLA lattice and lowered the melting peak by about 5 °C.

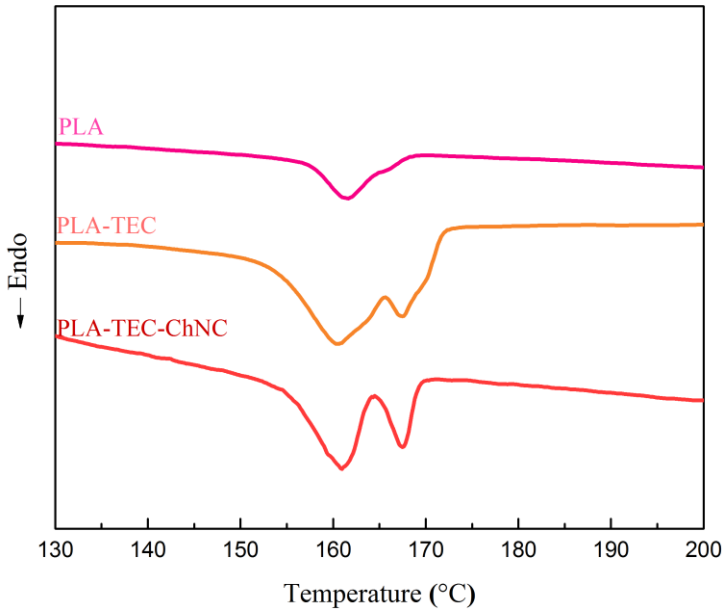

Figure 12. DSC heating scans of PLA, PLA-TEC, PLA-TEC-ChNC nanocomposite after isothermal crystallization at 125 °C for 30 min.

XRD measurements were performed to investigate the influence of ChNCs on the crystallization of PLA. Figure 13 shows comparative XRD graphs of PLA, PLA-TEC, and the PLA-TEC-ChNC nanocomposite. Strong diffraction rings appeared at 2θ = 12.3°, 14.7°, 16.7°, 19.0°, and 22.3°, which correspond to the (004)/(103), (010), (200)/(110), (203), and (015) crystallographic planes, respectively[36]. Among them, the strongest peak, observed at 16.7°, was assigned to the α-form of PLA[37]. In addition, some weak diffraction peaks were observed at 20.7°, 24.0°, 24.9°, 27.3°, 29.3°, and 31.1°. The peaks at 24.0° and 24.9° were ascribed to the α'-form of PLA[38].

Furthermore, the diffraction peak at 29.3° may have originated from the β-form of PLA, which is consistent with a previous finding[39] (2θ = 29.7° for the β-form of crystals). The peaks at 12.3° and 20.7° could be assigned to the D-form of PLA, since similar peaks at 2θ = 12.0° and 20.8° were reported by Han *et al.*[40] The XRD profile of PLA-TEC shows intense diffraction peaks, and it reveals that the intensity of the α-form of PLA was higher than that of its α'-form. The intensity of the peaks of PLA-TEC increased slightly with the incorporation of the ChNCs, and the positions of the peaks shifted to the left. The shift in the peak position suggests that PLA-TEC has a unit cell structure different from that of PLA; this, in turn, indicated that the incorporation of the ChNCs altered the crystal structure of PLA. The overall intensity of the peaks of the PLA-TEC-ChNC nanocomposite was higher than that of PLA-TEC. A total of three forms of PLA—the α-form, α'-form, and β-form—were observed.

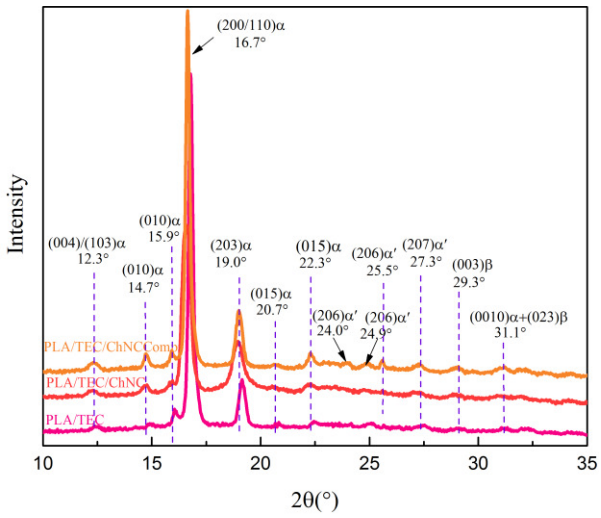

Figure 13. Comparative XRD graphs of isothermally crystallized PLA, PLA-TEC, and PLA-TEC-ChNC nanocomposite.

The crystal sizes of the materials were calculated using the Scherrer equation; the calculated data are listed in Table 3. The data revealed that the crystal size of PLA decreased in the presence of TEC and the ChNCs. The crystal size decreased from 46.87 nm (PLA) to 41.00 nm

(PLA-TEC). However, the crystal size reduced further with the incorporation of the ChNCs, to 32.53 nm. This reduction in the crystal size of PLA with the addition of ChNCs could have been caused by the good nucleation ability of the ChNCs. This hypothesis is consistent with the POM results, which revealed that the addition of ChNCs increased the nucleation density of PLA through a reduction in its crystal size.

Table 3. Comparison of crystal sizes of isothermally crystallized PLA, PLA-TEC, and PLA-TEC-ChNC nanocomposite with two intense peaks at 16.7° and 19.0°.

Materials	Crystal size (nm)	
	16.7° (peak 1)	19.0° (peak 2)
PLA	46.9	27.4
PLA-TEC	41.0	23.5
PLA-TEC-ChNC	32.5	20.6

Mechanism of improved crystallization by addition of ChNCs. We propose that the mechanism of the improved crystallization of plasticized PLA could be the H-bond interactions between PLA-TEC and the ChNCs, as shown in Figure 14. TEC has two types of functional groups: the acetyl functional group (-$OCOCH_3$) and the hydroxyl group (-OH). However, the acetamide group (-NH_2-CO-CH_3) and the hydroxyl group (-OH) on ChNCs have a better scope for interacting with the PLA chain. These functional groups on ChNCs can easily interact with the –C=O bond of PLA to achieve two types of H-bond interactions (-CO---OH and -CO--NH). These interactions are expected to be the cause of the improved crystallization of PLA in the presence of ChNCs; this belief is supported by the POM and DSC results.

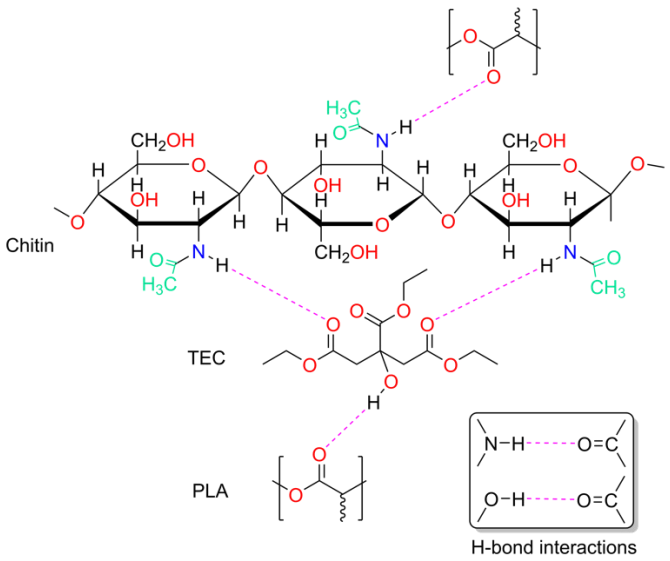

Figure 14. Schematic of mechanism of improved crystallization of PLA in the presence of ChNCs, showing two types of H-bond interactions.

The effect of addition of ChNCs on the interactions between the PLA chains and TEC was analyzed by FTIR spectroscopy. The FTIR spectra of PLA, PLA-TEC, and the PLA-TEC-ChNC nanocomposite are shown in Figure 15; the peaks at 2997 cm^{-1} and 2945 cm^{-1} in these spectra are ascribed to the asymmetric and symmetric stretching[41], respectively, of CH_3. However, the peak at 2881 cm^{-1} is ascribed to the –C-H stretching of CH_3. The peaks originate from 1759 cm^{-1} and 1188 cm^{-1} , respectively, the characteristic carbonyl (-C=O) and –C-O-C stretching of PLA[41]. The intensities of the C-O and C=O peaks increase with the addition of TEC and the ChNCs, and these peaks shift toward lower wavenumbers. Furthermore, weak peaks observed at 1658 cm^{-1} and 1619 cm^{-1} correspond to the amide I band of the acetamide group ($-NH_2-CO-CH_3$) of the chitins in the PLA-TEC-ChNC nanocomposites and the weak peak at 1558 cm^{-1} correspond to amide II band (*i.e.* N-H bending) of this acetamide group[42]. The peaks at 3265 cm^{-1} and 3110 cm^{-1} correspond to the -N-H stretching[43]. These results confirm the presence of ChNCs in the nanocomposite. The peak at 3504 cm^{-1} in PLA and that at 3504 cm^{-1} in PLA-TEC shift toward a

lower wavenumber (3498 cm^{-1}) with the addition of ChNCs to PLA-TEC. This result indicated the occurrence of H-bond interactions between PLA-TEC and ChNCs.

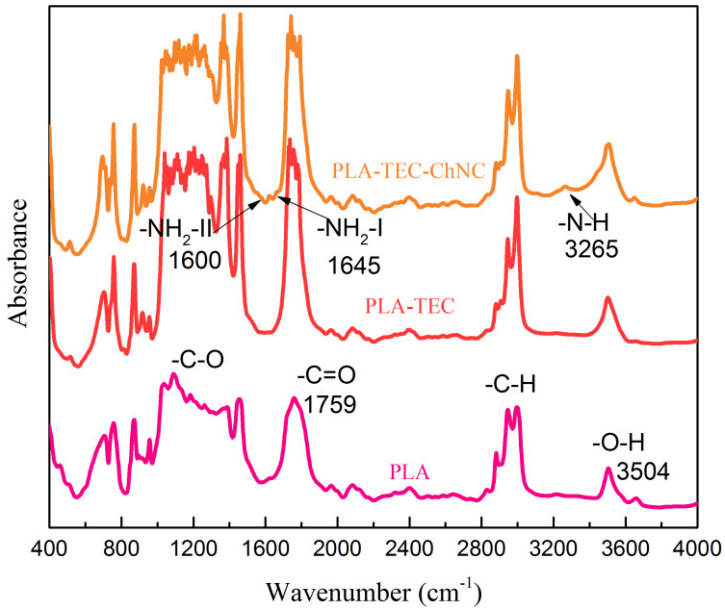

Figure 15. FTIR graphs of PLA, PLA-TEC, and PLA-TEC-ChNC nanocomposite, showing characteristic peaks of PLA and ChNCs. The graphs also depict the shifting of the O-H stretching peaks of PLA toward lower wavenumbers with the addition of ChNCs.

Crystallization kinetics of PLA-TEC and PLA-TEC-ChNC nanocomposite. The Lauritzen–Hoffman nucleation theory[44] was used to understand the effect of ChNCs on the crystallization of plasticized PLA and to study the crystallization kinetics. The crystal growth rate (G) at a specific crystallization temperature can be expressed using the Lauritzen–Hoffman equation as follows:

$$G = G_0 \exp\left(\frac{-U*}{R(T_c - T_\infty)}\right) exp\left(\frac{K_g}{T_c\ \Delta T_f}\right) \quad (3)$$

After simplification, equation 3 can be rewritten as

$$lnG + \frac{U^*}{R(T_c - T_\infty)} = \ln G_0 - \frac{K_g}{T_c\ \Delta T_f} \quad (4)$$

where G_0 is a pre-exponential factor and U^* is the activation energy required for the transportation of the polymer segments across the interfacial boundary between the melt and the crystals, and its value is 6280 J/mol. R is the gas constant; T_c is the isothermal crystallization temperature; and T_∞ is the temperature below which diffusion stops, and it usually equals to T_g - 30 K. Further, K_g is the nucleation constant; ΔT is the degree of supercooling, which is expressed as $\Delta T = T_m^o - T_c$; and f is a correction factor that denotes the change in the heat of fusion and is close to unity at high temperatures. $f = 2T_c/T_m^o + T_c$, where T_m^o is the equilibrium melting temperature and is the most important parameter for studying the crystallization kinetics. T_m^o values can be determined by extrapolating the experimentally observed melting temperatures by means of the Hoffmann–Weeks equation[45]. The values of T_m^o for PLA, PLA-TEC, and the PLA-TEC-ChNC nanocomposite were calculated by the Hoffmann–Weeks extrapolation[45]; the corresponding plots are shown in Figure 16, and the observed values are listed in Table 4. The value of nucleation constant for heterogonous or secondary nucleation can be calculated as follows:

$$K_g = \frac{nb\sigma\sigma_e}{\Delta H_f k} T_m^0 \quad (5)$$

where n is a constant whose value depends on the crystallization regime; b is the layer thickness, which is equal to 5.17×10^{-10}; σ and σ_e are the lateral and folding surface free energies, respectively; and k is the Boltzmann constant.

Table 4. Lauritzen–Hoffman parameters for isothermal crystallization of PLA, PLA-TEC, and PLA-TEC-ChNC nanocomposite.

Materials	T_m^o/°C	$K_g/k^2(10^5)$	σ_e/J $m^{-2}(10^{-2})$
PLA	184.9	8.7	1.8
PLA-TEC	176.3	2.1	0.5
PLA-TEC-ChNC	172.7	1.6	0.3

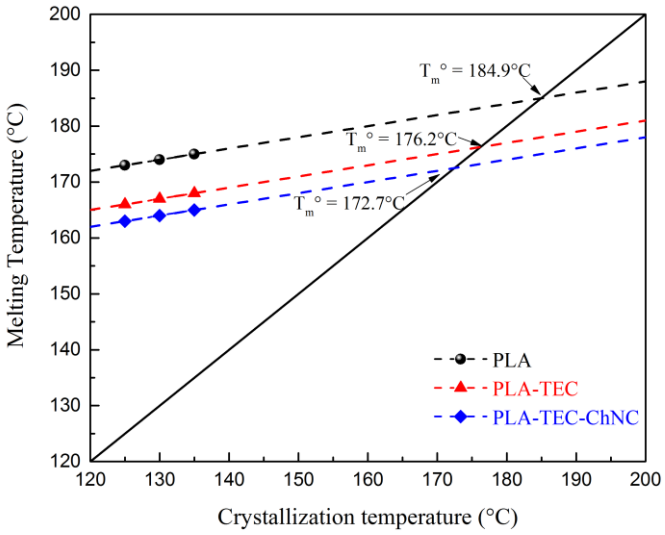

Figure 16. Determination of equilibrium melting temperature (T_m^o) of PLA, PLA-TEC, and PLA-TEC-ChNC nanocomposite by Hoffman–Weeks extrapolation.

Here, the growth rate (G) of all the materials was calculated by considering the spherulite growth as a function of time (see supporting information (S1–S6) for further details). The growth rate of spherulites can also be measured by observing the surface area covered with spherulites over a certain time duration (S7). The spherulite radius increased linearly with time, and G was calculated from the slopes of the fitted lines. Figure 17 shows the dependence of the spherulite growth rate on the isothermal crystallization temperature (T_c). The plots of $G + U^*/[R(T_c - T_\infty)]$ versus $10^5/(T_c \cdot \Delta T_f)$ for PLA, PLA-TEC, and the PLA-TEC-ChNC nanocomposite are shown in Figure 18; the K_g values were calculated from the slopes of the fitted lines and are listed in Table

4. It can be seen from Figure 18 that almost linear lines are obtained for all the materials. R^2 values for PLA, PLA-TEC, and the PLA-TEC-ChNC nanocomposite were 0.9489, 0.9959, and 0.9961, respectively. This result shows that the materials used in this study crystallize only in Regime II. Bai *et al.*[30] observed linear lines for PLA samples.

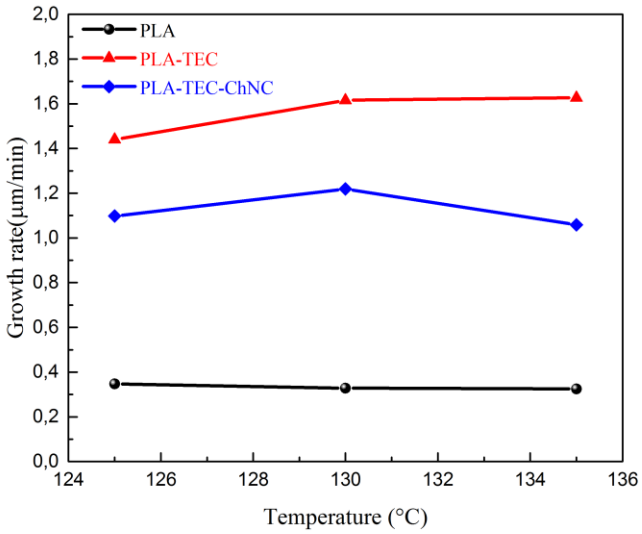

Figure 17. Estimation of spherulite growth rate (G) as a function of isothermal crystallization temperature (T_c) (125 °C, 130 °C, and 135 °C) for PLA, PLA-TEC, and PLA-TEC-ChNC nanocomposite.

Results of the Lauritzen–Hoffman analysis are presented in Table 4. It can be seen that the values of the nucleation constant (K_g) and surface free energy (σ_e) of PLA-TEC and the PLA-TEC-ChNC nanocomposite were decreased compared to those of PLA. These decreased values indicated that TEC and the ChNCs acted as barriers for primary nucleation.

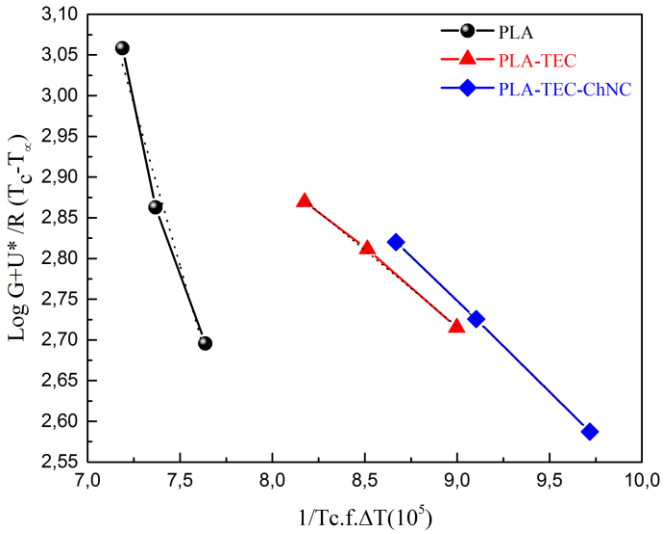

Figure 18. Lauritzen–Hoffman plots for PLA, PLA-TEC, and PLA-TEC-ChNC nanocomposite isothermally crystallized at designated temperatures.

CONCLUSIONS

A detailed study on the crystallization of plasticized PLA in the presence of ChNCs was conducted. The role of ChNCs in the crystallization was evaluated by POM, SEM, DSC, and XRD analyses. Additionally, FTIR spectroscopy was used to study the interaction between the components of PLA-TEC-ChNC nanocomposites, *i.e.*, *PLA*, TEC, and ChNCs. The crystallization rate of PLA was improved greatly by the addition of ChNCs. POM observations showed that the addition of ChNCs improved the crystallization rate of PLA and altered the morphology of the formed spherulites. Interestingly, ring-banded spherulites were formed at 130 °C, and rarely found neutral-type spherulites were also observed at 125 °C. The SEM study revealed an interesting nucleation effect of the ChNC nanoparticles on PLA-TEC, which resulted in different lamellar structures of spherulites. The DSC results showed that the T_g of PLA reduced upon addition of TEC, whereas it was comparatively higher after the addition of ChNC. This shows the good nucleation ability of the ChNCs. Additionally, the hump of the second

melting peak of in the PLA-TEC-ChNC nanocomposite were extremely prominent. The XRD results also confirmed the importance of the ChNCs, as some additional peaks were observed due to their presence. The Lauritzen–Hoffman nucleation theory revealed a decrease in the nucleation constant (K_g) and the surface free energy (σ_e) of PLA with the addition of ChNCs, indicating good nucleation ability of the ChNCs. Furthermore, knowledge of specific crystallization temperatures gained from this study can also be utilized during the processing of PLA-based nanocomposites to achieve films with better barrier and physical properties.

ACKNOWLEDGEMENTS

The authors are grateful for the financial support provided by the Joint European Doctoral Programme in Advanced Material Science and Engineering (DocMASE) to Shikha Singh. The authors would also like to thank Dr. Natalia Herrera and Dr. Shokat Sarmad for their technical assistance with the AFM and FT-IR spectroscopy studies.

REFERENCES

(1) Rafael A. Auras, Loong-Tak Lim, Susan E. M. Selke, H. T. *Poly(lactic acid): Synthesis, Structures, Properties, Processing, and Applications*; **2011**.

(2) Barrau, S.; Vanmansart, C.; Moreau, M.; Addad, A.; Stoclet, G.; Lefebvre, J.-M.; Seguela, R. *Macromolecules* **2011**, *44* (16), 6496–6502.

(3) Tang, H.; Chen, J. Bin; Wang, Y.; Xu, J. Z.; Hsiao, B. S.; Zhong, G. J.; Li, Z. M. *Biomacromolecules* **2012**, *13* (11), 3858–3867.

(4) Maiza, M.; Benaniba, M. T.; Quintard, G.; Massardier-Nageotte, V. *Polimeros* **2015**, *25* (6), 581–590.

(5) Kulinski, Z.; Piorkowska, E. *Polymer (Guildf).* **2005**, *46* (23), 10290–10300.

(6) Oksman, K.; Mathew, A. P.; Bondeson, D.; Kvien, I. *Compos. Sci. Technol.* **2006**, *66* (15), 2776–2784.

(7) Herrera, N.; Mathew, A. P.; Oksman, K. *Compos. Sci. Technol.* **2015**, *106*, 149–155.

(8) Ljungberg, N.; Wesslén, B. *Biomacromolecules* **2005**, *6* (3), 1789–1796.

(9) Maiza, M.; Benaniba, M. T.; Massardier-Nageotte, V. *J. Polym. Eng.* **2016**, *36* (4), 371–380.

(10) Labrecque, L. V; Kumar, R. A; Dave, V.; Gross, R. A; McCarthy, S. P. *J. Appl. Polym. Sci.* **1997**, *66* (8), 1507–1513.

(11) Pei, A.; Zhou, Q.; Berglund, L. A. *Compos. Sci. Technol.* **2010**, *70* (5), 815–821.

(12) Zaldua, N.; Mugica, A.; Zubitur, M.; Iturrospe, A.; Arbe, A.; Re, G. Lo; Raquez, J.-M.; Dubois, P.; Muller, A. J. *CrystEngComm* **2016**, *18* (48), 9334–9344.

(13) Mustapa, I. R.; Chandran, S.; Shanks, R. A.; Kong, I. In *Proceedings - 37th Annual Condensed Matter and Materials Meeting*; **2013**, 37, 23–26.

(14) Dong, W.; Ren, J.; Shi, D.; Ma, P.; Li, X.; Duan, F.; Ni, Z.; Chen, M. *Polym. Degrad. Stab.* **2013**, *98* (9), 1790–1795.

(15) Su, Z.; Li, Q.; Liu, Y.; Hu, G. H.; Wu, C. *J. Polym. Sci. Part B Polym. Phys.* **2009**, *47* (20), 1971–1980.

(16) Scaffaro, R.; Botta, L.; Lopresti, F.; Maio, A.; Sutera, F. *Cellulose*. **2017**, 447–478.

(17) Mathew, A. P.; Oksman, K.; Sain, M. *J. Appl. Polym. Sci.* **2006**, *101* (1), 300–310.

(18) Le Corre, D.; Bras, J.; Dufresne, A. *Biomacromolecules* **2010**, *11* (5), 1139–1153.

(19) Gray, D. G. *Cellulose* **2008**, *15* (2), 297–301.

(20) Sullivan, E. M.; Moon, R. J.; Kalaitzidou, K. *Materials (Basel).* **2015**, *8* (12), 8106–8116.

(21) Trifol, J.; Plackett, D.; Sillard, C.; Hassager, O.; Daugaard, A. E.; Bras, J.; Szabo, P. *J.*

Appl. Polym. Sci. **2016**, *133* (14).

(22) Oksman, K. *Handbook of Green Materials:Processing Technologies , Properties and Applications*; Word Scientific Publishing, **2014**.

(23) Herrera, N.; Salaberria, A. M.; Mathew, A. P.; Oksman, K. *Compos. Part A Appl. Sci. Manuf.* **2016**, *83*, 89–97.

(24) Herrera, N.; Roch, H.; Salaberria, A. M.; Pino-Orellana, M. A.; Labidi, J.; Fernandes, S. C. M.; Radic, D.; Leiva, A.; Oksman, K. *Mater. Des.* **2016**, *92*, 846–852.

(25) Xu, H.; Xie, L.; Jiang, X.; Li, X. J.; Li, Y.; Zhang, Z. J.; Zhong, G. J.; Li, Z. M. *J. Phys. Chem. B* **2014**, *118* (3), 812–823.

(26) Li, H.; Huneault, M. A. *Polymer (Guildf).* **2007**, *48* (23), 6855–6866.

(27) Langford, J. I.; Wilson, A. J. C. *J. Appl. Crystallogr.* **1978**, *11* (2), 102–113.

(28) Crist, B.; Schultz, J. M. *Prog. Polym. Sci.* **2016**, *56*, 1–63.

(29) Kalb, B.; Pennings, A. J. *Polymer (Guildf).* **1980**, *21* (6), 607–612.

(30) Bai, J.; Fang, H.; Zhang, Y.; Wang, Z. *CrystEngComm* **2014**, *16* (12), 2452.

(31) Ni'mah, H.; Woo, E. M.; Chang, S.-M. *RSC Adv.* **2014**, *4* (99), 56294–56301.

(32) Lim, L. T.; Auras, R.; Rubino, M. *Prog Polym Sci* **2008**, *33* (8), 820–852.

(33) Li, H.; Huneault, M. A. *Polymer (Guildf).* **2007**, *48* (23), 6855–6866.

(34) Li, C.; Liu, H.; Luo, B.; Wen, W.; He, L.; Liu, M.; Zhou, C. *Eur. Polym. J.* **2016**, *81*, 266–283.

(35) Muller, J.; Jiménez, A.; González-Martínez, C.; Chiralt, A. *Polym. Int.* **2016**, *65* (8), 970–978.

(36) Xu, J.-Z.; Chen, T.; Yang, C.-L.; Li, Z.-M.; Mao, Y.-M.; Zeng, B.-Q.; Hsiao, B. S. *Macromolecules* **2010**, *43* (11), 5000–5008.

(37) Pluta, M.; Galeski, A. *J. Appl. Polym. Sci.* **2002**, *86* (6), 1386–1395.

(38) Chen, X.; Kalish, J.; Hsu, S. L. *J. Polym. Sci. Part B Polym. Phys.* **2011**, *49* (20), 1446–1454.

(39) Sawai, D.; Takahashi, K.; Sasashige, A.; Kanamoto, T.; Hyon, S.-H. *Macromolecules* **2003**, *36* (10), 3601–3605.

(40) Han, L.; Pan, P.; Shan, G.; Bao, Y. *Polym. (United Kingdom)* **2015**, *63*, 144–153.

(41) Krikorian, V.; Pochan, D. J. *Macromolecules* **2005**, *38* (15), 6520–6527.

(42) Chen, C.; Li, D.; Hu, Q.; Wang, R. *Mater. Des.* **2014**, *56*, 1049–1056.

(43) Mathew, A. P.; Laborie, M. P. G.; Oksman, K. *Biomacromolecules* **2009**, *10* (6), 1627–1632.

(44) Lauritzen, J. I.; Hoffman, J. D. *J. Appl. Phys.* **1973**, *44* (10), 4340–4352.

(45) Marand, H.; Xu, J.; Srinivas, S. *Macromolecules* **1998**, *31* (23), 8219–8229.